ACS OMEGA

http://pubs.acs.org/journal/acsodf
Article

A Molecular Analogue of Cu/ZSM-5 Catalyzing the Monooxygenation of Hydrocarbons via a Mono μ-Oxo Dicopper Species

Alexander Stüber, Dmitry I. Sharapa, Felix Tuczek,* and Felix Studt*

Cite This: https://doi.org/10.1021/acsomega.6c00806
Read Online

ABSTRACT: The conversion of methane to methanol by the enzyme particulate methane monooxygenase (pMMO) represents an important sink in the global methane cycle. However, the exact molecular mechanism of the enzymatic reaction is unknown. An inorganic model system of pMMO is Cu/ZSM-5. There is experimental and theoretical evidence that the CH_4-to-CH_3OH conversion proceeds at a mono μ-oxo dicopper site in the latter system. We have prepared a discrete molecular complex exhibiting a Cu_2O core and found that it catalyzes the monooxygenation of aliphatic substrates with bond dissociation energies (BDEs) up to 82 kcal/mol. Herein, we show by theoretical calculations that this system exhibits an energy profile for the activation of C−H bonds that is comparable to that of Cu/ZSM-5 catalysts.

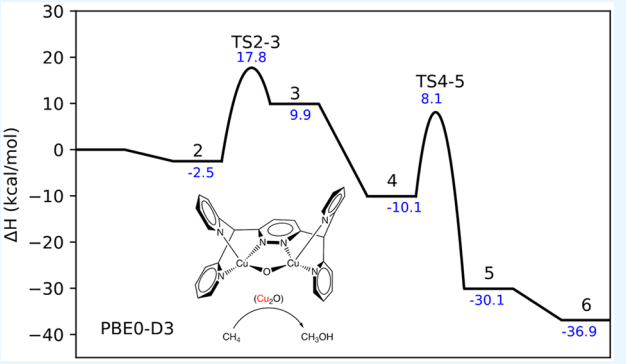

INTRODUCTION

After CO_2, methane is the second most abundant greenhouse gas. Although its atmospheric concentration is much lower than that of carbon dioxide, its global warming potential (GWP) is 2 orders of magnitude higher. The major part (about 60%) of the methane flux into the earth's atmosphere is due to agriculture, fossil fuel use, and other human activities. Natural sources of methane are wetlands, where methane is produced by microbes (methanogens), but methane emissions also derive from termites, oceans, and other sources. On the other hand, there are also microorganisms that feed on methane (methanotrophs), representing an important sink in the global methane cycle.

The first step of bacterial methane oxidation is mediated by enzymes converting methane to methanol (methane monooxygenases, MMOs). This reaction is particularly challenging as methane exhibits the strongest C−H bond of all hydrocarbons (C−H bond dissociation energy, BDE = 105 kcal/mol).[1,2] The way in which biological systems mediate direct methane oxidation under ambient conditions is thus of profound interest. For the iron-based, soluble form of MMO (sMMO), the corresponding mechanism has been elucidated, whereas for the more common, copper-dependent form of this enzyme (particulate MMO, pMMO), details of this reaction are still under debate.[3−8]

Over the years, two functional model systems of pMMO have been established. The first one, developed by Chan et al., is based on a trinuclear copper complex.[9,10] Upon reaction with O_2, two of the copper atoms form a Cu(II)−O-Cu(III) intermediate from the corresponding Cu(I) centers, being able to transfer one O atom to CH_4. The resulting Cu(I)···Cu(II) site is converted back to Cu(I)···Cu(I) with H_2O_2. Later, this system has been grafted to surfaces and optimized toward practical applications.[11,12] The second model system of pMMO is represented by a copper-containing zeolite, Cu/ZSM-5.[2,13,14] Monooxygenation of methane to methanol is mediated by a mono-μ-oxo dicopper (Cu(II)−O−Cu(II)) intermediate, which forms upon reaction of dioxygen (or N_2O) with two Cu(I) centers. These studies have also inspired a plethora of cation-exchanged zeolites mostly based on mono-, di-, and tricopper complexes that are anchored within the zeolite pores.[15]

To obtain further insight into the formation and monooxygenase reactivity of mono μ-oxo dicopper cores, we have recently synthesized two dinuclear copper complexes, $[Cu_2(bdpdz)]^{2+}$ based on 3,6-bis(di-2-pyridylmethyl)-pyridazine (bdpdz)[16] and $[Cu_2(bdptz)]^{2+}$ based on 1,4-bis(2,2′-dipyridylmethyl)phthalazine (bdptz)[17] ligands, both of which form mono μ-oxo dicopper cores upon reaction with oxygen atom transfer reagents or O_2.[18,19] Using a combination of resonance Raman and X-ray absorption spectroscopy (XAS)

Received: January 28, 2026
Revised: May 29, 2026
Accepted: June 1, 2026

as well as mass spectrometry, the fate of oxygen was monitored in these systems, from its initial binding to the copper centers to its final incorporation into aliphatic substrates.[19] Notably, Cu_2O species have been identified as reactive intermediates, mediating the oxygenation of hydrocarbons via H atom abstraction and subsequent oxygen transfer,[2,14,19] although this C−H bond activation could not be achieved for methane as this would require temperatures at which this system is not stable. Importantly, however, their atomic-scale structures are very similar to those postulated for Cu/ZSM-5,[2] (see Scheme 1).

Scheme 1. Structure of the Mono μ-Oxo Dicopper Intermediate of $[Cu_2(bdpdz)]^{2+}$ (1, left), and Copper-Doped ZSM-5 Zeolite (within 10-Membered Rings)

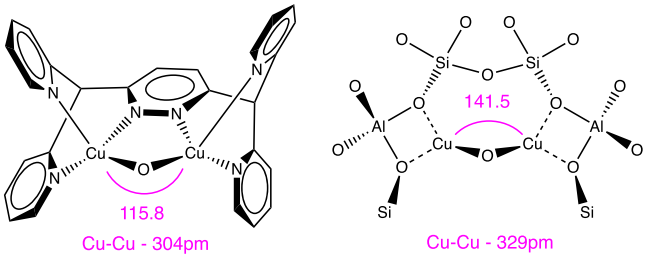

Although homogeneous systems allow monooxygenation reactions to be performed in a catalytic fashion, only substrates with a BDE of 82 kcal/mol or lower were found to be converted. In this context, it should be noted that the methane-to-methanol conversion with Cu/ZSM-5 requires elevated temperatures (150 °C)[2,13,14] whereas the Cu_2O intermediate of **1** is only stable up to room temperature. Moreover, the presence of surrounding solvent (in this case acetone, BDE = 99.5 kcal/mol by our calculation) practically limits the BDE of substrates that can be oxygenated with these systems. Nevertheless, in view of the close structural and electronic similarity of $[Cu_2(bdpdz)]^{2+}$ and $[Cu_2(bdptz)]^{2+}$ to the dicopper centers in Cu/ZSM-5, it is of high interest to theoretically evaluate the intrinsic activity toward C−H bond activation for both of these types of catalysts. To address this question, we have herein calculated energy profiles of C−H abstraction for various probe molecules and their further conversion to the corresponding alcohols on **1** with DFT, considering various organic substrates with calculated BDEs ranging from 85 kcal/mol (diphenylmethane) to 109 kcal/mol (methane, see the Supporting Information Table S5).

METHODS

DFT calculations were performed using the ORCA program package.[20] The PBE0 hybrid density functional was employed with the D3 Grimme dispersion correction (PBE0-D3)[21] in combination with the def2-TZVP basis set.[22] We employed the triplet dication state for the description of the two copper atoms in the Cu−O−Cu moiety. Upon reduction of the Cu−O−Cu moiety to Cu(I)−Cu(I), the system is calculated in the singlet ground state. Importantly, the triplet−singlet crossing occurring upon transformation of **3** to **4** (see below) is estimated to have a low barrier of 1.5 kcal/mol (more information is given in the Supporting Information). Starting from structure **4**, all further structures can be considered closed-shell singlets. All energies are zero-point energy (ZPE)-corrected, with vibrations being calculated using a partial Hessian (see the Supporting Information for details, a complete list of energies, geometries, and calculated vibrations). We also calculated the solvation energies of all species using SMD[23] as implemented in the ORCA code with acetone as the solvent. All solvation energies are given in Tables S3, S4, and S5.

Since theoretical studies in the literature regarding the use of copper-containing zeolites are typically based on GGA functionals (often PBE-D3), we also calculated important steps with the GGA-type PBE-D3[24,25] functional for comparison. Interestingly, PBE-D3 underestimates barrier heights by an average of 10 kcal/mol compared to PBE0-D3 (see the Supporting Information). We note, however, that given the different theoretical methods used herein, it is difficult to assess whether barriers are over- or underestimated. However, we note that the GGA-type PBE-D3 functional often underestimates reaction barriers, as also seen for zeolite chemistry.[26] We therefore believe that the barriers calculated with the hybrid PBE0-D3 functional provide a better estimate, as also highlighted by the comparison to available experimental data. A comparison of frontier orbitals derived from PBE-D3 and PBE0-D3 is given in Figures S6, S7, and S8.

RESULTS AND DISCUSSION

Considering the similar reactivity of $[Cu_2(bdpdz)]^{+2}$ and $[Cu_2(bdptz)]^{+2}$, we focused on the Cu_2O intermediate of the smaller model (**1**) and compared our results to those found for similar solid-state systems, such as Cu/ZSM-5.[15] While it is experimentally not possible to evaluate the activation of methane on complex **1** (see above), we aim here at shedding light on the reactive potential of **1** and, in particular, on the comparison to Cu/ZSM-5. Figure 1 shows the calculated

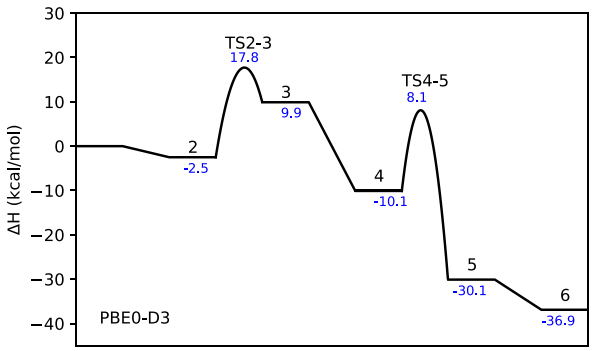

Figure 1. Calculated ZPE-corrected reaction enthalpy diagram of the activation of methane over **1**. Structures and optimized geometries of the intermediates **2**−**5** and transition states **TS2-3** and **TS3-4** are shown in Scheme 2 and Figure 2, respectively. All energies are given relative to the gas-phase species and complex **1**. The step 5 → 6 is depicting the exchange of methanol with acetone; a specific barrier for this has not been calculated.

energy profile of methane activation on complex **1** and the subsequent conversion to methanol; the structures and optimized geometries are shown in Scheme 2 and Figure 2. As can be seen from Figure 1, methane adsorption to **1** leading to **2** is slightly exothermic, mostly due to dispersion interactions between **1** and the substrate. Activation of the C−H bond of methane is accompanied by an activation barrier of 20.3 kcal/mol when measured to adsorbed methane (**2**). Interestingly, the geometry of the transition state (**TS2-3**) has O−H and H−C bond lengths of 1.213 and 1.307 Å, respectively, with the CH_3 radical floating above the activated hydrogen atom (cf. Figure 2). This transition-state geometry is in close analogy to that calculated for Cu/ZSM-5.[2]

The final state of the C−H activation process is the formation of the O−H bond and a CH_3 radical that is physisorbed on top of the hydrogen atom (**3**) in a geometry

https://doi.org/10.1021/acsomega.6c00806
ACS Omega XXXX, XXX, XXX−XXX

Scheme 2. Structures of 1 with the Transition State of H Abstraction (TS2-3), the Interaction with the Methyl Radical (3), Methyl Bound to Copper (4) after Crossing to the Singlet Ground State, the Transition State of C−O Coupling (TS4-5) to Produce Adsorbed Methanol (5), and with (6) Showing the Complex with Adsorbed Acetone

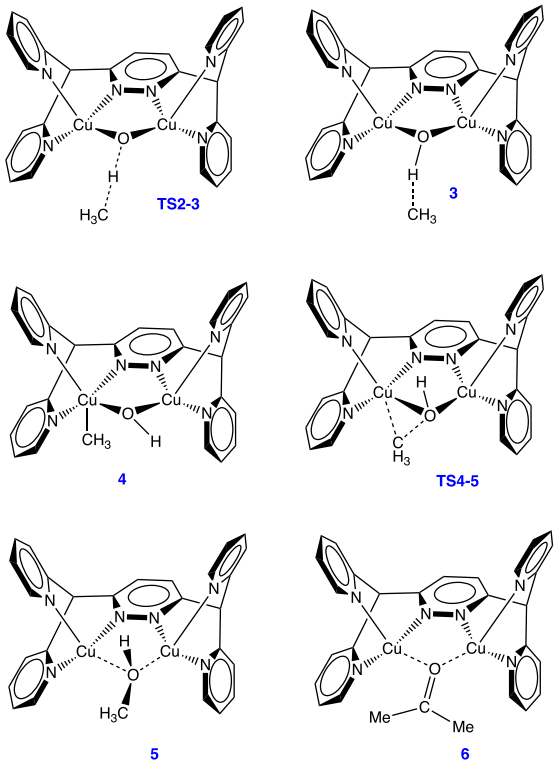

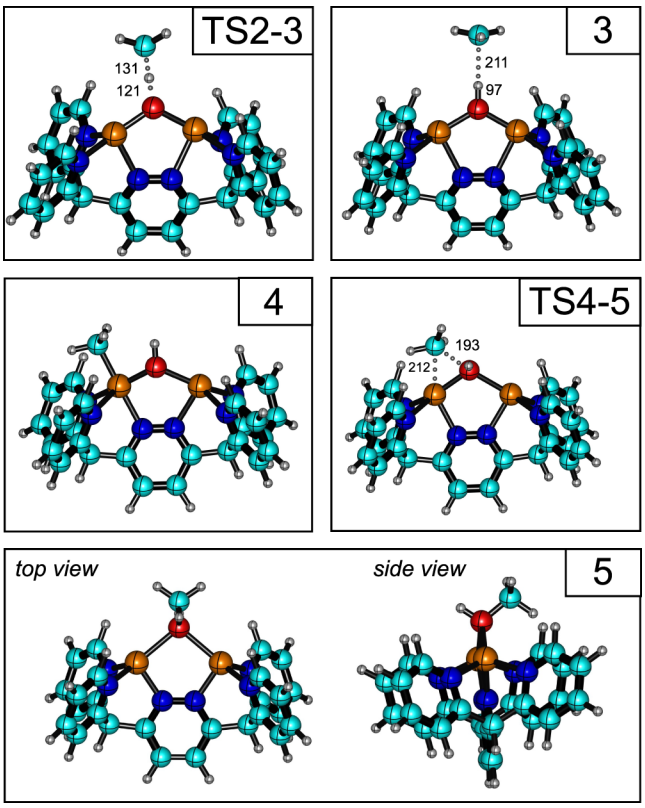

Figure 2. Optimized geometries of **TS2-3**, **3**, **4**, **sTS4-5**, and **5**. Cu atoms are depicted in orange, oxygen in red, nitrogen in blue, carbon in cyan, and hydrogen in gray. Distances for the most interesting O−H and C−H bonds are given in pm.

that is very similar to the preceding transition state **TS2-3**. This process is calculated to be 12.4 kcal/mol uphill in energy when referenced to adsorbed methane (**2**; 9.9 kcal/mol with respect to the gas phase (**1**)), with both the geometry and energy strikingly similar to those obtained for Cu/ZSM-5. Note that intermediate **3** is calculated to be in a triplet state. Its subsequent transformation to a singlet state (**4**) is exothermic by 20.0 kcal/mol and accompanied by the movement of the CH_3 group to bind to one of the copper atoms. The corresponding spin crossover is associated with a small barrier that we calculated to be 1.7 kcal/mol using the NEB method UKS (see Figure S5 and the corresponding discussion for details). We used minimum-energy crossing point (MECP) optimization for finding the conical intersection between **3** and **4**, and this conical intersection was (logically) found to be very close to **3** (see the Supporting Information for more details).

The reaction proceeds via oxygen insertion into the Cu−C bond to yield methanol coordinated between two copper atoms (**5**) with an energy barrier of 18.2 kcal/mol when referenced to the preceding state (**4**). Finally, methanol bound to the two copper atoms is exchanged with the solvent acetone, yielding **6**, being downhill by 6.8 kcal/mol. Note that the adsorption of methanol in **5** is −74.7 kcal/mol when referenced to methanol in the gas phase, as it is coordinated to two copper atoms.

From the described computational results, we conclude that the activation of methane over **1** follows a very similar mechanism to the one calculated for Cu/ZSM-5, both in terms of energetics and geometries. This also emerges from a quantitative comparison of our results with literature data on the methane-to-methanol conversion over Cu/ZSM-5 (Table 1). Note that we also calculated the important steps of the pathway using the GGA PBE-D3 functional (cf. Table 1; see the Supporting Information for details) to have a better comparison with literature data that used PBE or other GGA functionals.

When comparing the activation barrier of the hydrogen atom transfer to the Cu−O−Cu moiety, we find that this barrier has been experimentally determined to be 15.7 kcal/mol for Cu−O−Cu in MFI, with calculated values ranging from 16.3 to 22.2 kcal/mol, depending on the employed functional and active-site motif (Table 1). Interestingly, the adsorption of the formed methanol (**5**) is quite a bit stronger on **1** compared to that found for the Cu−O−Cu zeolites. The corresponding barrier (**TS4-5**), however, is similar. The high binding of product methanol prevents its overoxidation. For the solid-state systems, however, liberation of the formed methanol requires a stepwise process,[14,15] whereas in the homogeneous system, the formed alcohols are further oxidized to the corresponding ketones in a follow-up reaction.[19]

For comparison, we also investigated C−H bond activation at compound **1** for four additional organic molecules, namely, propane, toluene, diphenylmethane (DPM), and acetone, which is the solvent used in the above homogeneously catalyzed process. Figure 3 shows the optimized geometries of C−H bond activation; the energetics are given in Figure 4 and Table S3. As can be seen from Figure 4, the adsorption becomes stronger when going from methane to propane, toluene, DPM, and finally acetone. We attribute this to

https://doi.org/10.1021/acsomega.6c00806
ACS Omega XXXX, XXX, XXX−XXX

Table 1. Energies (kcal/mol) with Respect to the Methane-Adsorbed State (2), Calculated for $CH_4 \rightarrow CH_3OH$ at Cu in Compound 1 and Zeolites

ref.	activ. barrier 2 → 3	CH_3 radical (3)	trans. state 4 → 5	bound CH_3OH (5)	functional	remark
this work	20.3	12.4	18.2	−27.6	PBE0-D3	
	9.8	8.9			PBE-D3	
[2]	18.5	∼14			B3LYP	calc. ZSM-5
[2]	15.7					expt. ZSM-5
[27]	14.8	9.0		−17.5	BEEF-vdW	mordenite
[28]	16.3	13.1	19.6	−14.2	PBE-D2	mordenite
[29]	19.6/10.4	−18.5	0	∼−23	PBE	ZSM-5 adsorbed state at 0
[30]	22.2	15.4	?	−12.4	PBE	ZSM-5

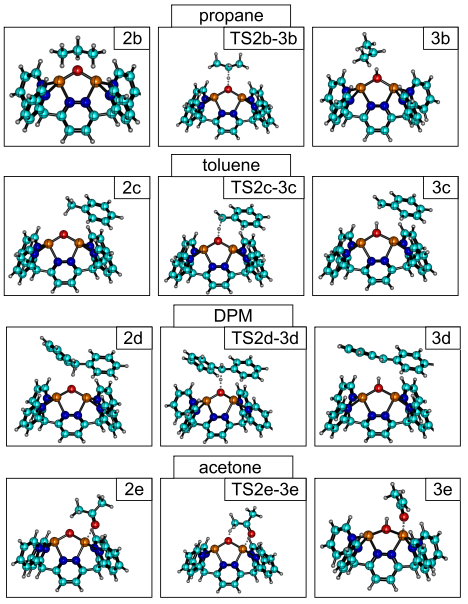

Figure 3. Geometries of optimized initial states (ISs), transition states (TSs), and final states (FSs) of propane, toluene, acetone, and DPM with dicopper complex **1**.

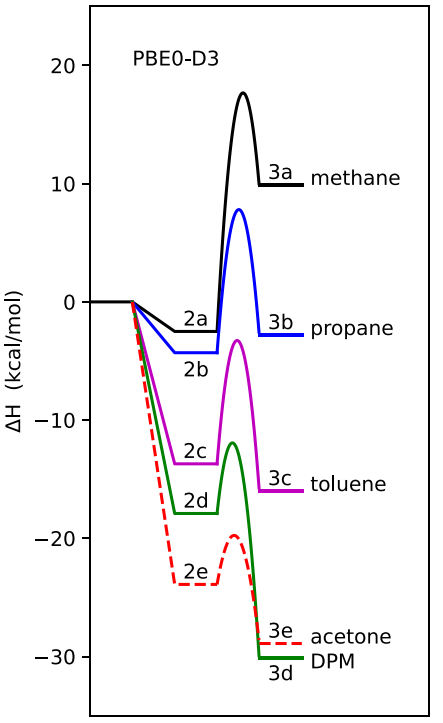

Figure 4. Calculated enthalpies of the activation of methane (black), propane (blue), toluene (magenta), diphenylmethane (DPM, green), and acetone (red) over **1**. All enthalpies are given in kcal/mol and referenced to the reactant molecule in the gas phase.

increased vdW interactions with an increasing size of the adsorbate. Our calculated transition-state energies (see Figure 3 for structures) are 7.8, −3.3, −11.8, and −20.0 kcal/mol for propane, toluene, DPM, and acetone, respectively, when referenced to the corresponding molecule in the gas phase. Note that the final-state energies (see Figure 3 for structures) also decrease in a similar manner going from −2.8 (propane), −16.0 (toluene), and −30.1 (DPM) to −28.9 kcal/mol (acetone). While C−H bond activation thus follows a similar pattern to that observed for methane, one obvious outlier is represented by acetone (which has been used as a solvent in the experimental investigations). C−H activation of acetone differs markedly as it coordinates strongly to one of the copper atoms in the initial, transition, and final states, thus deviating from all other investigated molecules.

Since C−H bond activation of methane, propane, toluene, and DPM seems to follow a very similar pattern, we investigated whether there are correlations between transition-state energies and the C−H bond strength (also given by the BDE) as has been observed in previous studies of C−H activation by copper-containing complexes.[31]

Figure 5 shows the calculated transition-state enthalpies for methane, propane, toluene, DPM, and acetone over **1** as a function of their calculated BDEs. Note that the transition-state enthalpy is referenced to the gas-phase species (H^{act})

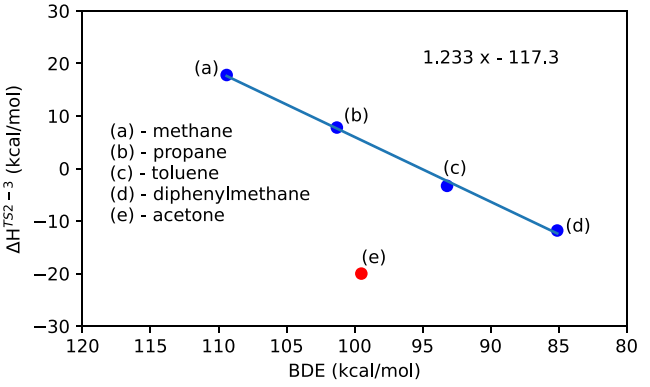

Figure 5. Calculated transition-state enthalpies of C−H activation for methane, propane, toluene, diphenylmethane, and acetone over **1** as a function of their calculated bond dissociation energies (BDEs). All energies are given in kcal/mol and referenced to the reactant molecules in the gas phase.

https://doi.org/10.1021/acsomega.6c00806
ACS Omega XXXX, XXX, XXX−XXX

rather than their adsorbed counterpart to avoid complications arising from the adsorption enthalpies of the molecules. As can be seen from Figure 5, there is a remarkable correlation between the transition-state enthalpy of C−H activation and the BDE, with the notable exception of acetone, as one might expect from the rather different structure. In fact, excluding acetone, the correlation has a mean absolute error (MAE) of only 0.5 kcal/mol. We thus conclude that any molecule that follows a similar activation pattern as methane should fall on this line and one only needs to know its BDE to estimate the activation energy. Note also that from our analysis, DPM has a very low value of the transition-state enthalpy of −12.4 kcal/mol, corresponding to an activation enthalpy of +6.2 kcal/mol when measured relative to the initial state with adsorbed DPM. For 9,10-dihydroanthracene (BDE = 81 kcal/mol), which has been used in the experiments,[19] we estimate a transition-state energy of −17.4 kcal/mol based on the scaling relationship in Figure 5. Because of this, we failed to calculate the actual transition-state geometry as the potential energy landscape around this point is extremely flat. This, in turn, would correspond to a practically barrierless reaction (see the Supporting Information for an in-depth discussion of this issue).

CONCLUSIONS

To conclude, we used calculated DFT data on the C−H activation of methane to compare Cu/ZSM-5 to complex **1**. Considering the transition state for methane activation, **1** lies at 17.8 and 20.3 kcal/mol when referenced to gas-phase and adsorbed methane, respectively, which is very similar to the solid-state system. Experimentally, this barrier has been determined to be 15.7 kcal/mol, whereas DFT calculations give 18.5 kcal/mol for Cu-ZSM-5 when referenced to the adsorbed state.[2] Note, however, that DFT calculations vary from 10.3 to 22.2 kcal/mol,[28−30,32] with hybrid functionals usually yielding higher barriers, as we also found when comparing PBE0-D3 with PBE-D3 (about 10 kcal/mol difference). In practice, this reactive potential of **1** cannot be exploited as this complex is subject to thermal decay above room temperature and thus cannot be heated to the temperatures applied for the methane-to-methanol conversion over Cu/ZSM-5 (about 150 °C). Moreover, being a homogeneous system, the solvent would be attacked by the catalyst under these conditions. Finally, the above analysis has been conducted for a "naked" Cu_2O moiety, whereas in homogeneous solution, the copper centers of this core may be coordinated by other (e.g., solvent) molecules. If such additional ligands are taken into account, both the activation energy (**TS2-3**) of the hydrogen atom transfer step and the energy of the formed alkyl radical (3) increase by up to 5 kcal/mol, depending on the ligand (cf. Table S6 and Figure S6). On the other hand, the methane-to-methanol conversion over Cu/ZSM-5 only proceeds stoichiometrically; i.e., this system has to be reoxidized after every oxygenation run, whereas the catalytically active species **1** in the Cu-bdpdz system is regenerated from O_2 after oxygen transfer to the substrate(s), closing the catalytic cycle.[19] Although the TONs achieved for the monooxygenation of aliphatic substrates on the basis of **1** have been low to date, the activity of such systems may be increased by suitable modification of the catalyst design.[33]

ASSOCIATED CONTENT

Supporting Information

The Supporting Information is available free of charge at https://pubs.acs.org/doi/10.1021/acsomega.6c00806.

PBE coordinates (ZIP)

DFT and CASSCF calculations, description of methodology of thermochemistry calculation based on partial Hessians, tables with absolute and relative energies of different species, and coordinates of all species mentioned in this manuscript including systems with adsorbed solvents (PDF)

AUTHOR INFORMATION

Corresponding Authors

Felix Tuczek − *Institute of Inorganic Chemistry, Christian-Albrechts-University, Kiel 24098, Germany;* orcid.org/0000-0001-7290-9553; Email: ftuczek@ac.uni-kiel.de

Felix Studt − *Institute of Catalysis Research and Technology, Karlsruhe Institute of Technology, Eggenstein-Leopoldshafen 76344, Germany; Institute for Chemical Technology and Polymer Chemistry, Karlsruhe Institute of Technology, Karlsruhe 76131, Germany;* orcid.org/0000-0001-6841-4232; Email: felix.studt@kit.edu

Authors

Alexander Stüber − *Institute of Inorganic Chemistry, Christian-Albrechts-University, Kiel 24098, Germany*

Dmitry I. Sharapa − *Institute of Catalysis Research and Technology, Karlsruhe Institute of Technology, Eggenstein-Leopoldshafen 76344, Germany*

Complete contact information is available at: https://pubs.acs.org/10.1021/acsomega.6c00806

Author Contributions

All authors have given approval to the final version of the manuscript.

Notes

The authors declare no competing financial interest.

ACKNOWLEDGMENTS

D.I.S. and F.S. acknowledge funding by the Deutsche Forschungsgemeinschaft (DFG, German Research Foundation) − SFB 1441 − Project-ID 426888090 (project B4). The authors acknowledge support by the state of Baden-Württemberg through bwHPC and the German Research Foundation (DFG) through grant no. INST 40/575-1 FUGG (JUSTUS 2 cluster, RVs bw17D011). Financial support from the Helmholtz Association, Germany is also gratefully acknowledged.

ABBREVIATIONS

DFT-density functional theory
GWP-global warming potential
MMO-methane monooxygenases
bdpdz-3,6-bis(di-2-pyridylmethyl)pyridazine
bdptz-1,4-bis-(2,2′-dipyridylmethyl)-phthalazine
DPM-diphenylmethane
ZSM-5-zeolite socony mobil-5, an aluminosilicate of the pentasil zeolite family
BDE-bond dissociation energy

https://doi.org/10.1021/acsomega.6c00806
ACS Omega XXXX, XXX, XXX−XXX

TON-turnover number
MAE-mean absolute error
MFI-mordenite framework inverted
vdW-van der Waals

REFERENCES

(1) Blanksby, S. J.; Ellison, G. B. Bond dissociation energies of organic molecules. *Acc. Chem. Res.* **2003**, *36* (4), 255−263.
(2) Woertink, J. S.; Smeets, P. J.; Groothaert, M. H.; Vance, M. A.; Sels, B. F.; Schoonheydt, R. A.; Solomon, E. I. A Cu2O2+ core in Cu-ZSM-5, the active site in the oxidation of methane to methanol. *Proc. Natl. Acad. Sci. U.S.A.* **2009**, *106* (45), 18908−18913.
(3) Merkx, M.; Kopp, D. A.; Sazinsky, M. H.; Blazyk, J. L.; Müller, J.; Lippard, S. J. Dioxygen Activation and Methane Hydroxylation by Soluble Methane Monooxygenase: A Tale of Two Irons and Three Proteins. *Angew. Chem., Int. Ed.* **2001**, *40* (15), 2782−2807.
(4) Koo, C. W.; Tucci, F. J.; He, Y.; Rosenzweig, A. C. Recovery of particulate methane monooxygenase structure and activity in a lipid bilayer. *Science* **2022**, *375* (6586), 1287−1291.
(5) Peng, W.; Qu, X.; Shaik, S.; Wang, B. Deciphering the oxygen activation mechanism at the CuC site of particulate methane monooxygenase. *Nat. Catal.* **2021**, *4* (4), 266−273.
(6) Solomon, E. I.; Heppner, D. E.; Johnston, E. M.; Ginsbach, J. W.; Cirera, J.; Qayyum, M.; Kieber-Emmons, M. T.; Kjaergaard, C. H.; Hadt, R. G.; Tian, L. Copper active sites in biology. *Chem. Rev.* **2014**, *114* (7), 3659−3853.
(7) Koo, C. W.; Rosenzweig, A. C. Biochemistry of aerobic biological methane oxidation. *Chem. Soc. Rev.* **2021**, *50* (5), 3424−3436.
(8) Ross, M. O.; Rosenzweig, A. C. A tale of two methane monooxygenases. *J. Biol. Inorg. Chem.* **2017**, *22* (2−3), 307−319.
(9) Chen, P. P.-Y.; Yang, R. B.-G.; Lee, J. C.-M.; Chan, S. I. Facile O-atom insertion into C-C and C-H bonds by a trinuclear copper complex designed to harness a singlet oxene. *Proc. Natl. Acad. Sci. U.S.A.* **2007**, *104* (37), 14570−14575.
(10) Chan, S. I.; Lu, Y.-J.; Nagababu, P.; Maji, S.; Hung, M.-C.; Lee, M. M.; Hsu, I.-J.; Minh, P. D.; Lai, J. C.-H.; Ng, K. Y.; Ramalingam, S.; Yu, S. S.-F.; Chan, M. K. Efficient oxidation of methane to methanol by dioxygen mediated by tricopper clusters. *Angew. Chem., Int. Ed.* **2013**, *52* (13), 3731−3735.
(11) Liu, C.-C.; Mou, C.-Y.; Yu, S. S.-F.; Chan, S. I. Heterogeneous formulation of the tricopper complex for efficient catalytic conversion of methane into methanol at ambient temperature and pressure. *Energy Environ. Sci.* **2016**, *9* (4), 1361−1374.
(12) Liu, C.-C.; Janmanchi, D.; Wen, D.-R.; Oung, J.-N.; Mou, C.-Y.; Yu, S. S.-F.; Chan, S. I. Catalytic Oxidation of Light Alkanes Mediated at Room Temperature by a Tricopper Cluster Complex Immobilized in Mesoporous Silica Nanoparticles. *ACS Sustainable Chem. Eng.* **2018**, *6* (4), 5431−5440.
(13) Groothaert, M. H.; Smeets, P. J.; Sels, B. F.; Jacobs, P. A.; Schoonheydt, R. A. Selective oxidation of methane by the bis(mu-oxo)dicopper core stabilized on ZSM-5 and mordenite zeolites. *J. Am. Chem. Soc.* **2005**, *127* (5), 1394−1395.
(14) Snyder, B. E. R.; Bols, M. L.; Schoonheydt, R. A.; Sels, B. F.; Solomon, E. I. Iron and Copper Active Sites in Zeolites and Their Correlation to Metalloenzymes. *Chem. Rev.* **2018**, *118* (5), 2718−2768.
(15) Kulkarni, A. R.; Zhao, Z.-J.; Siahrostami, S.; Nørskov, J. K.; Studt, F. Cation-exchanged zeolites for the selective oxidation of methane to methanol. *Catal. Sci. Technol.* **2018**, *8* (1), 114−123.
(16) Manzur, J.; García, A. M.; Letelier, R.; Spodine, E.; Peña, O.; Grandjean, D.; Olmstead, M. M.; Noll, B. C. Synthesis and magnetostructural characterization of dinuclear copper(II) complexes with the diazine ligand, 3,6-bis(di-2-pyridylmethyl)pyridazine. *J. Chem. Soc., Dalton Trans.* **1993**, *6*, 905−911.
(17) Barrios, A. M.; Lippard, S. J. Amide Hydrolysis Effected by a Hydroxo-Bridged Dinickel(II) Complex: Insights into the Mechanism of Urease. *J. Am. Chem. Soc.* **1999**, *121* (50), 11751−11757.
(18) Haack, P.; Limberg, C. Molecular Cu(II)-O-Cu(II) complexes: still waters run deep. *Angew. Chem., Int. Ed.* **2014**, *53* (17), 4282−4293.
(19) Jurgeleit, R.; Grimm-Lebsanft, B.; Flöser, B. M.; Teubner, M.; Buchenau, S.; Senft, L.; Hoffmann, J.; Naumova, M.; Näther, C.; Ivanović-Burmazović, I.; Rübhausen, M.; Tuczek, F. Catalytic Oxygenation of Hydrocarbons by Mono-μ-oxo Dicopper(II) Species Resulting from O-O Cleavage of Tetranuclear CuI /CuII Peroxo Complexes. *Angew. Chem., Int. Ed.* **2021**, *60* (25), 14154−14162.
(20) Neese, F. Software update: The ORCA program system—Version 5.0. *Wiley Interdiscip. Rev.: Comput. Mol. Sci.* **2022**, *12* (5), No. e1606.
(21) Adamo, C.; Barone, V. Toward reliable density functional methods without adjustable parameters: The PBE0 model. *J. Chem. Phys.* **1999**, *110* (13), 6158−6170.
(22) Weigend, F.; Ahlrichs, R. Balanced basis sets of split valence, triple zeta valence and quadruple zeta valence quality for H to Rn: Design and assessment of accuracy. *Phys. Chem. Chem. Phys.* **2005**, *7* (18), 3297−3305.
(23) Marenich, A. V.; Cramer, C. J.; Truhlar, D. G. Universal solvation model based on solute electron density and on a continuum model of the solvent defined by the bulk dielectric constant and atomic surface tensions. *J. Phys. Chem. B* **2009**, *113* (18), 6378−6396.
(24) Becke, A. D.; Johnson, E. R. A density-functional model of the dispersion interaction. *J. Chem. Phys.* **2005**, *123* (15), No. 154101.
(25) Perdew, J. P.; Burke, K.; Ernzerhof, M. Generalized Gradient Approximation Made Simple. *Phys. Rev. Lett.* **1996**, *77* (18), 3865−3868.
(26) Plessow, P. N.; Studt, F. How Accurately Do Approximate Density Functionals Predict Trends in Acidic Zeolite Catalysis? *J. Phys. Chem. Lett.* **2020**, *11* (11), 4305−4310.
(27) Xu, J.; Liu, B. Modeling C−H Bond Activation and Oxidations of Alkanes over Cu−MOR Using First-Principles Methods. *J. Phys. Chem. C* **2019**, *123* (16), 10356−10366.
(28) Mahyuddin, M. H.; Staykov, A.; Shiota, Y.; Miyanishi, M.; Yoshizawa, K. Roles of Zeolite Confinement and Cu−O−Cu Angle on the Direct Conversion of Methane to Methanol by [Cu 2 (μ-O)] 2+ -Exchanged AEI, CHA, AFX, and MFI Zeolites. *ACS Catal.* **2017**, *7* (6), 3741−3751.
(29) Arvidsson, A. A.; Zhdanov, V. P.; Carlsson, P.-A.; Grönbeck, H.; Hellman, A. Metal dimer sites in ZSM-5 zeolite for methane-to-methanol conversion from first-principles kinetic modelling: is the [Cu−O−Cu] 2+ motif relevant for Ni, Co, Fe, Ag, and Au? *Catal. Sci. Technol.* **2017**, *7* (7), 1470−1477.
(30) Li, G.; Vassilev, P.; Sanchez-Sanchez, M.; Lercher, J. A.; Hensen, E. J.; Pidko, E. A. Stability and reactivity of copper oxo-clusters in ZSM-5 zeolite for selective methane oxidation to methanol. *J. Catal.* **2016**, *338*, 305−312.
(31) Latimer, A. A.; Kulkarni, A. R.; Aljama, H.; Montoya, J. H.; Yoo, J. S.; Tsai, C.; Abild-Pedersen, F.; Studt, F.; Nørskov, J. K. Understanding trends in C-H bond activation in heterogeneous catalysis. *Nat. Mater.* **2017**, *16* (2), 225−229.
(32) Yumura, T.; Hirose, Y.; Wakasugi, T.; Kuroda, Y.; Kobayashi, H. Roles of Water Molecules in Modulating the Reactivity of Dioxygen-Bound Cu-ZSM-5 toward Methane: A Theoretical Prediction. *ACS Catal.* **2016**, *6* (4), 2487−2495.
(33) Stüber, A.; Jurgeleit, R.; Grimm-Lebsanft, B.; Buchenau, S.; Kellner, I.; Appiarius, Y.; Näther, C.; Krahmer, J.; Ivanović-Burmazović, I.; Rübhausen, M.; Naumova, M. A.; Tuczek, F. Dinuclear Copper Complex with a Pyridazine-Bridged Octadentate Ligand: Monooxygenase Activity and Characterization of Copper-Oxygen Intermediates. *Chemistry (Weinheim an der Bergstrasse, Germany)* **2025**, *31*, No. e202501659.

https://doi.org/10.1021/acsomega.6c00806
ACS Omega XXXX, XXX, XXX−XXX